Finding optimal geometries for noise barrier tops using scaled experiments

Sergey I. Voropayev[a)]
Department of Civil and Environmental Engineering and Earth Sciences
University of Notre Dame, Notre Dame, IN 46556

Nicholas C. Ovenden[b)]
Department of Mathematics, University College London
Gower Street, London WC1E 6BT, United Kingdom

Harindra J. S. Fernando
Department of Civil and Environmental Engineering and Earth Sciences
Department of Aerospace and Mechanical Engineering
University of Notre Dame, Notre Dame, IN 46556

Paul R. Donovan
Illingworth-Rodkin Inc.
1 Willowbrook Court, Suite 120
Petaluma, CA 94954

[a)]Professor Sergey Voropayev passed away on 30th June 2016 after a short battle with cancer. May his Soul Rest in Peace.

[b)]Corresponding Author. Email: n.ovenden@ucl.ac.uk

Abstract

Scaled acoustic laboratory experiments are used to develop a methodology for obtaining the acoustic characteristics of different barrier top designs and for identifying geometries that may have advantages over the traditional thin vertical screen. The idea is to use a short impulsive spherical sound pulse possessing a broad frequency spectrum. If the duration of the pulse is sufficiently short, the entire primary signal, which travels by the shortest direct route diffracting at the top of the barrier, arrives at the receiver much earlier than any secondary signals reflected from the surroundings. Secondary signals may therefore be ignored and only the information from the primary signal can be analysed. When the typical frequency band of the sound pulse is about an order of magnitude higher than typical traffic noise spectra, then scaled acoustic modeling using the same scaling factor for lengths and distances is possible. The results of such experiments are reported here for barriers with six different geometries. Using spectral analysis, insertion losses as functions of frequency were calculated for different source-receiver positions and barrier tops. The results were then rescaled for full-size traffic barriers and, using a typical traffic noise spectrum, single number ratings of barrier performance were obtained.

Keywords: scaled experiments; noise barrier design; impulsive sound source; diffraction.

I. Introduction

Traffic noise barriers are widely used to reduce exposure to traffic noise in neighbouring residential areas. In the presence of a barrier, the noise at a receiver location on the opposite side of the barrier from a source is due to two sound pathways: the transmitted pathway through the barrier and the diffracted waves emanating from the top of a barrier. Barriers are usually built with solid materials that should effectively block direct sound propagation. However, it is known that poorly fitted panels and other defects can lead to *sound leaks* that significantly reduce barrier performance in the field[1]. Such construction-related performance issues and the transmitted pathway are not considered in this paper. A solid barrier's performance is thus limited by the diffracted sound which is highly dependent on (i) source frequency, (ii) relative source and receiver positions and (iii) the barrier top geometry[2].

The simplest way to improve barrier performance at a given receiver location is to increase its height. However, aesthetic problems as well as cost and safety issues usually prevent the transportation authorities from increasing the height of barriers above a certain limit[3]. Since different barrier top geometries modify the diffracted waves, various barrier shapes have been investigated in an attempt to achieve the same performance as a higher vertical screen . By finding an improved barrier top design it may be possible to keep the same barrier performance with a reduced barrier height.

In recent decades, numerous modifications to barrier design have been proposed to improve barrier performance and there are now a number of different designs of barrier top used in practice. For instance, in Japan alone there are approximately 20 types of devices that modify the edge shape of the noise barrier and are distributed as commercial products[4,5]. Shapes of different barrier tops have included T-shaped, L-shaped, Y-shaped, as well as arrow, cylindrical, multiple and random edge configurations.

Different methods are used to study top-modified barriers. They include field and large scale measurements, theoretical/numerical simulations and scaled laboratory experiments. Field measurements are complicated, expensive, have poorly controlled background conditions and are usually difficult to repeat and interpret[6,7], while large scale experiments require huge anechoic laboratories which are expensive to build and run. The main problem in three-dimensional simulations is the long calculation time, especially for barriers with complicated tops and so, often, the calculations are carried out using a two-dimensional model. Two-dimensional boundary element methods have been used to estimate the insertion loss of noise barriers. Numerical models have been developed to calculate barrier efficiency, to assess the acoustic performance of a range of barrier designs and for optimization of the acoustic performance of barriers[8–10]. Finite-element methods are also used to calculate the insertion loss of different noise barrier designs[11]. The computational cost for these two-dimensional numerical simulations is not significant but the cost increases significantly for fully three-dimensional calculations and for higher frequencies. The calculation time depends also on some other parameters, *e.g.* the chosen frequency range[12,13].

While some of the difficulties in conducting field experiments have been addressed by the new European procedure EN 1793-4:2015 (previously CEN/TS 1793-4)[14], an experimental method in which scaled experiments are used offers an attractive alternative[15,16]. The main idea of this approach is based on the invariance of the sound speed in air for similar field and laboratory conditions. This allows a scaled model of the barrier to mimic the performance of a real traffic barrier, when the frequency band of the laboratory sound source is increased by the same factor relative to typical frequency band of traffic noise. The scaling is straightforward if any surfaces reacting with the measured sound are rigid, otherwise the impedance of the surfaces must also be scaled. The scaled

approach is readily adopted in the present communication as we focus purely on the optimal diffractive properties of various barrier top geometries, which are assumed to be rigid throughout.

The main purpose of this present work is to develop a universal methodology for obtaining the diffractive characteristics of different top barrier designs and, by comparison, identify geometries that may have performance advantages over traditional thin screen barriers. Our approach is to use scaled laboratory experiments and an impulsive point sound source. If the duration of the sound pulse is sufficiently short, the primary signal that takes the shortest most direct route diffracts above barrier and arrives at the receiver much earlier than any secondary signal that has been reflected or diffracted by the surroundings. These latter signals are easily separated from the primary signal infomation and only the information from the primary signal is analysed. Such an approach eliminates the need to build an expensive acoustic anechoic chamber for experiments, thus paving a new avenue for conducting acoustic experiments in the laboratory. The apparatus is placed in the laboratory on a dense, thick wood table that serves as the ground plane. The typical frequency range of the sound source (1–30 kHz) is 10 times the typical frequency range of traffic noise (100–3000 Hz). Thus the experiments can be considered as 1:10 scaled experiments of a real traffic noise barrier top.

The barriers top designs considered in this paper can be divided into two groups: (i) barriers with homogeneous tops that maintain the same height and geometry along the entire barrier length and (ii) barriers with heterogeneous tops that have variable height and geometry along the barrier length. Typical examples of homogenous tops include a thin vertical screen and T-shape tops. Typical examples of heterogeneous tops are the so-called jagged tops which have a regular or random variation of height and geometry. Naturally, the acoustic diffractive characteristics of the homogeneous barrier tops remain uniform

along the barrier, while for heterogeneous barriers it changes along the barrier and this complicates the measurements and interpretation (see below).

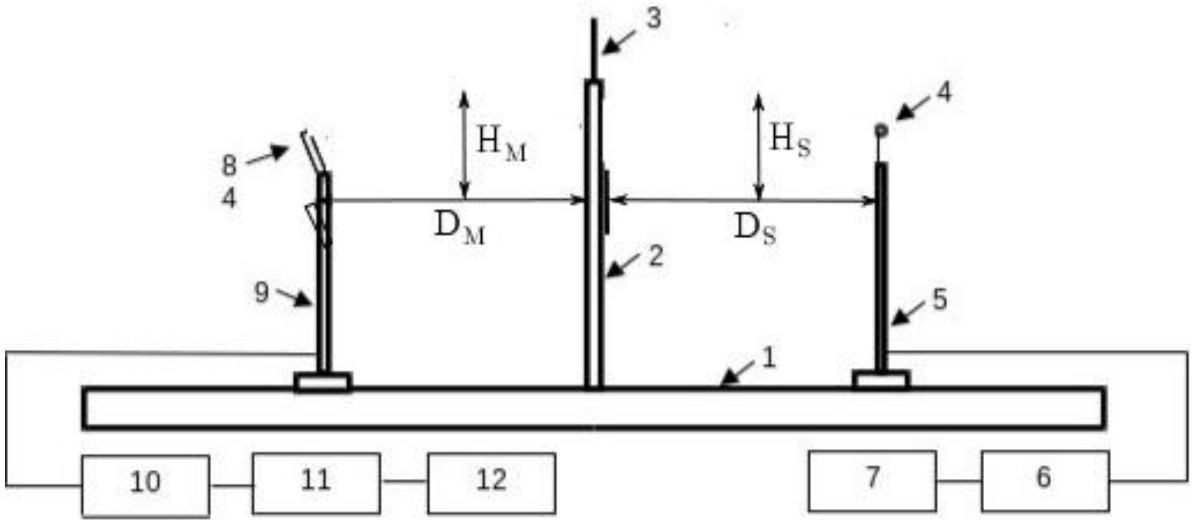

Figure 1: Experimental schematic and instruments.1 - large solid wood table, 2 - vertical wooden barrier, 3 - removable aluminum top attached to the barrier, 4 - impulsive sound source fixed to support 5, 6 - high voltage source for main electrodes, 7 - high voltage source for trigger electrode, 8 - microphone with preamplifier fixed under grazing angle to support 9, 10 - microphone conditioning amplifier, 11 - 100 MHz digital storage oscilloscope, 12 - computer with LabVIEW software.

II. Experimental set-up and method

A. Experimental schematic and instrumentation

Experiments were conducted in a laboratory in air at room temperature; see Fig. 1 for a schematic. The experimental apparatus consists of: (1) a large solid wooden table, (2) a vertical wooden barrier (2.5cm × 60cm × 120cm) with (3) removable aluminum plates

(0.15cm × 15cm × 120cm) with different top geometries, (4) an impulsive sound source fixed to a support (5), (6) a high voltage source for the main electrodes, (7) a high voltage source for the trigger electrode, (8) a Brüel & Kjær (type 4939-A-011) 1/4" free-field microphone with preamplifier 2670 and TEDS fixed below the grazing angle to support (9), (10) a Brüel & Kjær (type 2690-A-0S1) microphone conditioning amplifier, (11) a Tektronix (type 2230) 100 MHz digital storage oscilloscope, (12) a computer with LabVIEW software to analyze and store the measured signals. After each experiment the measured signals were post processed using the custom built MATLAB software described in appendix A.

B. Laboratory sound source

In experiments related to scaled acoustic modeling, different methods are used to model an impulsive point source with a short spherical acoustic wave of high intensity. Gun shots, the discharge of shot-shell primers, ultrasonic air-jet whistles, very powerful impulse lasers and spark dischargers have all been used to produce short N-shaped spherical sound waves[17–21]. The most popular method to generate an N-shaped sound wave is to use a spark discharger and there are a number of descriptions of different spark dischargers in the literature. These descriptions, however, are only schematics that omit the important details required to build such a device[22,23]. As a consequence, we designed and constructed our own device ab initio, taking into account the following main requirements: relative simplicity, short duration, small size, omnidirectionality and most importantly - high stability. To satisfy these requirements and by taking into account that two-electrode devices are typically not stable, a three-electrode triggered spark discharger was built, as shown in Fig 2.

The electrodes are made from tungsten rods with pointed ends. Two main electrodes (diameter 0.3 cm) and a third triggering electrode (diameter 0.15 cm) are fixed to three bronze holders (diameter 0.5 cm, length 15 cm) on a plastic support and attached to a tripod. The gap between main electrodes (0.0-1.0 cm), as well as the position of trigger

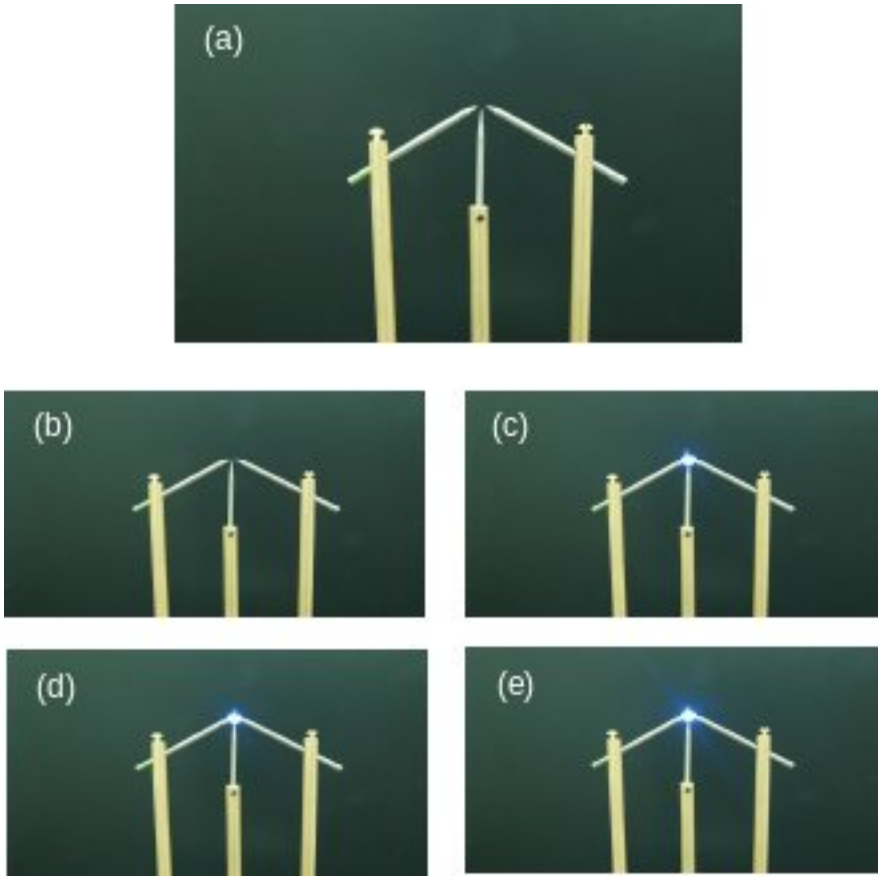

Figure 2: The sound source: (a) – three spark discharger electrodes on bronze supports are shown, the central smaller trigger electrode is between two main electrodes; (b) – a small trigger spark between trigger (central) and two main electrodes; (c) the main single spark between two main electrodes; (d) – two and (e) – four sparks at one exposure. Good spark repeatability is obvious. In this example the electrode gap is 0.3 cm and a high voltage 3 kV is used.

electrode, can be adjusted.

The sparks were generated by first applying a high voltage (3-5 kV depending on the gap) between the two main electrodes. This voltage was produced by a variable six stage Cockcroft-Walton voltage multiplier circuit and was kept lower than the breakdown voltage of the gap. After that, a short impulse of smaller voltage (1-2 kV depending on the trigger electrode position) was applied to the third trigger electrode placed between two main electrodes to provide an initial ionization of the air necessary to cause the spark breakdown and subsequent discharge of the capacitors in the voltage multiplier. After the spark was discharged, the capacitors were recharged and after a short time the next spark was able to be generated. Voltage measurements were made with a high-voltage probe (1000:1) placed on the high-voltage electrodes and showed high stability ($\pm 0.03\%$ variability) with time (see appendix B for further details).

The most important sound source characteristics are: (i) repeatability of sound wave duration and intensity, and (ii) approximate omnidirectionality at the very least. These properties were confirmed for our spark discharger by our measurements. Test measurements were made for two microphone orientations - normal to the sound wave front and at grazing angle. Comparison showed that although the microphone sensitivity is higher in the normal position, its transitional characteristics and omnidirectionality are improved when in the grazing position. This is in agreement with available data and is related to the specific construction of condenser microphones. In addition, the microphone safety grid generates a diffracted signal that contaminates the measured signal in the normal microphone position. Taking this into account, the grazing position was chosen as the primary microphone position in all measurements.

Typical traces of the recorded pressure $P(t)$ (measured in Pascals) as a function of time, t, for the grazing microphone position are given in Fig. 3(a). These data were

obtained with an interval between traces of about 1 min in the absence of a barrier (the free, F, signal) at a distance of 90 cm between the microphone and sound source. All seven signals recorded practically collapse onto a single curve and thus very good short-time stability and trigger synchronization are observed. The long-time stability was also satisfactory. After hundreds of sparks the signals remain practically indistinguishable from the data shown in Fig. 3 and no electrode cleaning was necessary.

The data for free signal shown in Fig. 3(a) gives an estimate of $T = 60\mu$s for the typical signal duration and thus the dominant frequency is determined as $f_0 = 1/T \approx 17$kHz. At normal atmospheric conditions this gives an estimate of $L = 2$cm for the typical wave length, which may be used as a characteristic length scale, *e.g.*, for the lateral variations in the jagged barrier top profiles (see below). The distance between the main electrodes (0.3 cm) is much less than L and so the sound source can be regarded as a point source at the typical distances of about 60-90 cm which were used between the microphone and sound source in our experiments. The azimuthal distribution of the sound intensity for the grazing microphone position is shown in Fig. 3(b) and the distribution appears to be approximately omnidirectional.

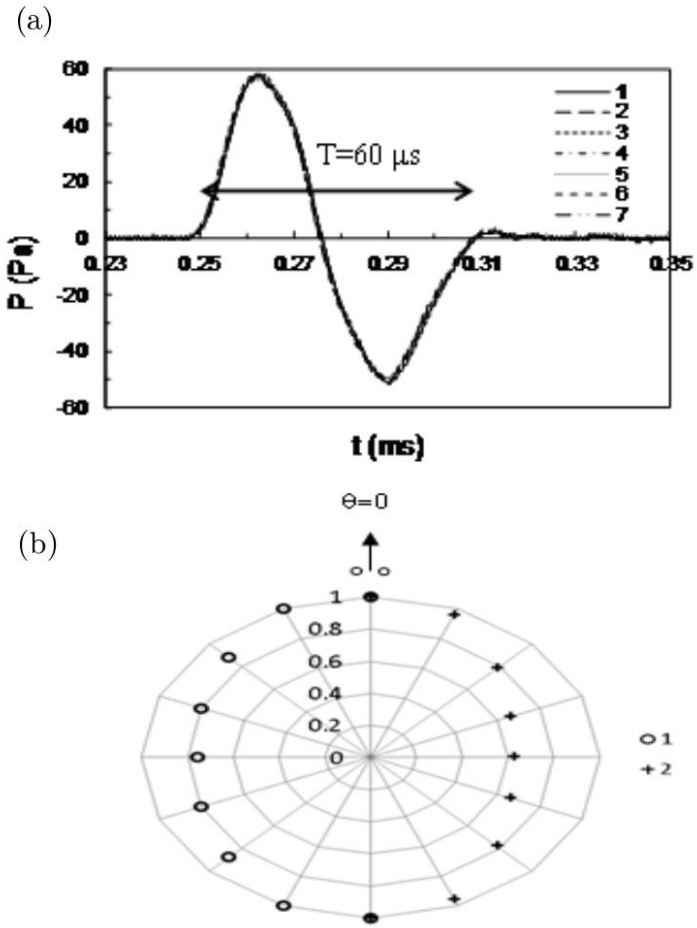

Figure 3: (a) the sound pressure, $P(t)$, in the absence of barrier (free, F, signal) as a function of time, t, for grazing microphone position at a distance of 90 cm between the microphone and sound source. Seven records are shown (see legend). In this example, the electrode gap is 0.3 cm and the high voltage is 3 kV. The typical signal duration is $T = 60\mu$s. (b) normalized azimuthal distributions of the maximum positive (1) and negative (2) sound pressure for the grazing microphone position. Direction $\theta = 0$ is shown by the arrow, and main electrodes are shown by two small circles near the arrow.

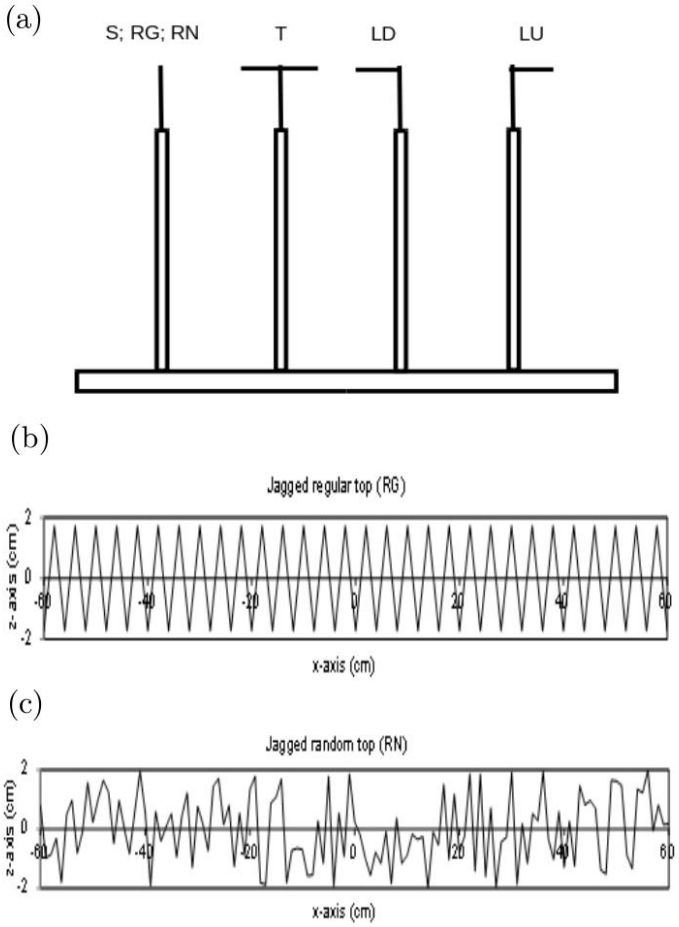

Figure 4: (a) The barrier top geometries used in the experiments: thin vertical screen (S), jagged regular (RG), jagged random (RN), T-shape (T), L-shape extending away from the sound source (LD), L-shape extending towards sound source (LU). The source is located to the right of the barrier and the microphone is to the left; (b) the jagged regular barrier top lateral profile (RG); (c) the jagged random (RN) barrier top lateral profile. All other geometries (S), (T), (LD) and (LU) simply coincide with the line $z = 0$.

C. Measurements procedure

In experiments, the large solid wooden table (5cm × 150cm × 450cm) served as the ground. A vertical barrier was fixed rigidly to the table and various removable aluminum tops, all of which could be moved accurately along the barrier, were attached to the barrier. Six different tops were used in this study as shown in Fig. 4: a thin vertical screen with a straight top (S), jagged regular (RG), jagged random (RN), T-shape (T), L-shape down (LD) extending away from the source, and L-shape up (LU) extending towards the source. All tops were made from aluminum and were considered to be acoustically rigid and non-absorbing.

For the jagged regular geometry (RG) a system of identical triangles with equal horizontal, Δx, and vertical, Δz, spacing was used; the jagged random geometry (RN), on the other hand, had a piecewise profile with fixed horizontal spacing, Δx, but with a randomly generated vertical spacing of mean value Δz. These geometries are shown in Fig. 4(b) and 4(c) respectively. The choice of spacing, 2 cm, was dictated by the characteristic wave length of the sound source. For L-shape and T-shape profiles, one or two aluminum 5×5 cm L-shape corners were attached to the vertical aluminum plate. Hence, the T-shape top had a 10 cm long horizontal section and each L-shape top had a 5cm long horizontal section. The mean vertical top position (set at $z = 0$) was identical for all top profiles.

The microphone and sound source positions relative to the barrier are shown in Fig. 5. In experiments the distance R from the barrier top (30 or 45 cm) was fixed, but angles, θ_S and θ_M, were varied. For the microphone four different angles were used, $\theta_M = 0°$, $15°$, $30°$, $45°$, and two different angles were used for the sound source, $\theta_S = 15°$, $30°$. Thus, for each of the six top geometries (S, T, LU, LD, RG, RN) shown in Fig. 4 and for one set with the free (F) signal (no barrier), eight sets of experiments with different θ_S and θ_M values were conducted at two values of distance R; thus, in total, $7 \times 8 \times 2 = 112$

experiments were performed. All measurements were made with the vertical plane passing through both the microphone and sound source lying normal to the barrier. For convenience, the notation S−−M−−R−− is used below for the various source-microphone positions. For example, S15M00R30, means that $\theta_S = 15°$, $\theta_M = 0°$ and $R = 30$cm.

In experiments where the top geometry did not vary along the barrier (homogeneous tops), three measurements at each microphone-source position were made and averaged data were used for processing. In experiments using RG and RN, where the top geometry varied along the barrier, a set of measurements performed at different barrier locations was conducted by sliding the aluminium top along the upper part of the wooden barrier between recordings. A fine ruler permitted us to measure accurately the change in barrier position x between recordings as shown in Fig. 4(b) and 4(c). Overall for RG and RN, seventeen measurements were made at $x = 0$, ± 0.5, ± 1.0, ... ± 4.0 cm for each top.

The experiments were conducted as follows. The microphone and sound source were fixed at a selected position as in Fig. 5. Firstly, the free (F) direct signal (with no barrier) was measured three times to check repeatability. Thereafter, the barrier was installed with the microphone and sound source remaining in the same positions, although the microphone was slightly corrected to the new grazing angle relative to the barrier top. Then, different removable aluminum tops were attached to the barrier: thin vertical screen (S), T-shape (T), L-shape up (LU), L-shape down (LD), jagged regular (RG) and then jagged random (RN) tops were used in succession and the data on the diffracted signals were obtained.

As schematically shown in Fig. 1, the free signal or diffracted signal from the barrier top arrives at the microphone with preamplifier and goes to the conditioning amplifier with variable amplification and frequency window 0.1–10^5 Hz. The typical signal amplitude is of the order of 3–6 V. This signal is displayed on the 100 MHz digital storage oscilloscope

screen and digitized at a selected frequency. In all measurements this frequency was set to $f_S = 2$ MHz, which enabled 4000 data points to be stored with the time interval $\Delta t = 0.5\mu$s. To omit the secondary diffracted/reflected signals that arrive at later times ($t > 1.5$ms) reflected from the barrier sides, ground and room ceiling/walls, only the first $N_0 = 3000$ data points were used.

A series of sixteen experiments with different sound source-microphone positions (see Fig. 5) were conducted. For each position the following set of 7 experiments was made: (i) - free signal (F) was measured 3 times; (ii) - diffracted signal from homogeneous tops (S, T, LU, LD) was measured 3 times, (iii) - diffracted signal from jagged tops (RG, RN) was measured 17 times at different x-positions, as explained above. After visual analysis, the digital data from the oscilloscope memory were transported to the computer with LabVIEW software and stored in separate files.

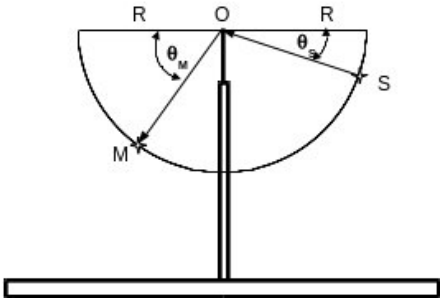

Figure 5: Schematic showing microphone, M, sound source, S, and angles, θ_M and θ_S, relative to the horizontal line passing through the origin, O, which coincides with the top of the barrier. The microphone and the sound source are at the same distance, $R = 30$ or 45 cm, from the origin and the angles used are: $\theta_S = 15°$, $30°$, $\theta_M = 0°$, $15°$, $30°$, $45°$.

D. Post-processing procedure

After each experiment, the measured sound pressure signals stored by the LabVIEW software were post processed using custom-built MATLAB software (see Appendix A). Methods of spectral analysis were used in the data processing. First, the pressure frequency spectra were calculated from the initial sound pressure data. After that, additional functions were used to calculate insertion losses for different tops as functions of the frequency and of the source and microphone positions. Using the insertion loss functions, the results were rescaled to spatial dimensions comparable to a full-size noise barrier and frequencies were rescaled to values typical for traffic noise sources. Single number ratings of the traffic barrier performance were then calculated and directivity diagrams obtained.

Two different methods were used to calculate the frequency spectra, namely, a standard fast Fourier transform (FFT) and a 1/3rd octave filter. In the FFT method, to improve the resolution, the spectral window width was reduced by using standard zero padding and thus an additional 17000 points were added to the original $N_0 = 3000$ data points; thus, in total, $N_T = 20000$ points were used in the FFT calculations. For the spectral window width this yields the estimate $\Delta f = f_S/N_T = 100$Hz, which remains constant across the entire frequency band. Calculations were made only in the frequency range 600–50000 Hz which are the scaled frequencies relevant for traffic noise. In the 1/3rd octave filter method we used a spectral filter developed by Couvreur[24], which was modified to cover a higher frequency band (up to 80 kHz). Calculations of insertion losses were made with standard central frequencies in the range 630–50000 Hz and the window width increasing with frequency. Note that the calculation here is not the same as averaging the FFT calculations over 1/3rd octave windows. Instead, a completely different direct filter method was used and the results obtained by standard FFT with a constant window width and the 1/3 Octave filter are compared below.

In the FFT method, first, the complex frequency spectrum of the sound pressure is calculated and the spectral density amplitude $S(f)$ is then determined by the magnitude of this frequency spectrum, where $f = 600, 700, 800, \ldots, 50000$ Hz. In the 1/3rd octave filter method the spectral density amplitude $S(f)$ is calculated directly at the standard 1/3rd octave central frequencies $f = 630, 800, 1000, \ldots, 50000$ Hz.

Using the spectral density amplitudes, the values of the insertion loss functions may be calculated as

$$IL(f) = 10 \log_{10} |S_0(f)/S(f)| , \tag{1}$$

where S_0 is the spectral density amplitude of the free (F) signal and $S(f)$ is the spectral density amplitude obtained when one of the barrier types is positioned between the source and microphone. Note that the definition of insertion loss gives the *relative* sound attenuations for different frequencies and these attenuations *do not* depend directly on the characteristics of the sound source used in the experiment. This permits the use of short sound pulses in testing barrier performance alone as mentioned in the introduction.

Because the sound pressure of the diffracted signal is a function of many parameters, the spectral density amplitude and insertion loss are also functions of those parameters. Thus,

$$IL = IL(f, R, \theta_S, \theta_M, A, x), \tag{2}$$

where R, θ_S, θ_M describe the source and microphone positions, A is the barrier top type (S,T,LD, LU, etc.) and x is the dependence on the lateral barrier position for the non-homogeneous tops RG and RN. In this way, insertion losses for the different barrier top geometries can be calculated and their performance compared.

Naturally, the main purpose of such scaled experiments is to measure the actual insertion loss functions for full size noise barriers. If the typical sound source frequency in the experiments is N times the frequency of the traffic noise (in our case $N = 10$, see

below), the experiments can be considered as a $1:N$ scaled experiments. The frequency of the laboratory measured insertion loss function is simply rescaled from the laboratory frequency f to the traffic noise frequency as $F = f/N$. Then, using the rescaled insertion loss function and proper estimates for the free traffic noise spectrum, the characteristics of the diffracted traffic noise behind a barrier with a rescaled length scale can be estimated. In particular, a single number rating for the traffic barrier performance can be estimated and the directivity diagrams obtained for different barrier tops.

III. Diffraction theory

The insertion loss function for the simplest case of the thin vertical screen straight top barrier can be parameterized in terms of the Fresnel number, $\mathcal{F}_N$. This number is the most important dimensionless parameter affecting the diffracted signal in the considered geometry (Fig. 5) and can be defined for our case as

$$\mathcal{F}_N = \frac{4Rf}{C}\left(1 - \sqrt{\frac{1+\cos(\theta_M+\theta_S)}{2}}\right)\cos\left(\frac{\theta_M-\theta_S}{2}\right) \tag{3}$$

where C is the ambient speed of sound. Based on the experiments reported by Maekawa[25], the following empirical parameterization for the insertion loss (in dB) of vertical thin screens is proposed[26,27]:

$$\mathrm{IL} = a_0 + 20\log_{10}\frac{\sqrt{2\pi\mathcal{F}_N}}{\tanh\sqrt{2\pi\mathcal{F}_N}}, \tag{4}$$

where a_0 is an empirical constant. Maekawa's estimate (4) for a thin vertical screen is shown as a dotted line in some plots of insertion loss presented in Section V.

A more accurate validation of the experimental results obtained in the laboratory is to compare the measured insertion losses obtained for each 1/3rd octave frequency band to those obtained using the so-called geometrical theory of diffraction. The analytical solution adopted for this purpose is that of wave diffraction by a wedge[28,29]. We adopt the input

parameters as shown in Fig. 5. Unlike other insertion loss calculations for noise barriers[30,31], here we only take into consideration the primary signal from the shortest ray of distance $2R$. The contributions of all other possible rays that are reflected at least once off the ground or off some other object are ignored. This assumption is valid given the shortness of the incident pulse as discussed in the previous section. For a point source of frequency f in a non- refracting atmosphere of constant sound speed C, the pressure field measured at the microphone situated behind a thin vertical screen is

$$p_{\mathrm{mic}} = \frac{\mathrm{e}^{+\mathrm{i}\pi/4}}{\sqrt{2}} \left[A_D\left(\sqrt{\frac{2kR}{\pi}}\cos\left(\frac{\theta_S-\theta_M}{2}\right)\right) + A_D\left(\sqrt{\frac{2kR}{\pi}}\sin\left(\frac{\theta_S+\theta_M}{2}\right)\right)\right] \frac{\mathrm{e}^{+\mathrm{i}k2R}}{2R}, \quad (5)$$

where $k = 2\pi f/C$ and the function $A_D(X)$ governing the diffraction behaviour[28] can be written as the integral

$$A_D(X) = \frac{1}{\sqrt{2}\pi}\int_{-\infty}^{+\infty} \frac{\mathrm{e}^{-u^2}\,\mathrm{d}u}{\left[X\sqrt{\pi/2} - \mathrm{e}^{-\mathrm{i}\pi/4}\,u\right]}. \quad (6)$$

For calculation purposes, it is more convenient to express $A_D(X)$ in terms of the auxiliary Fresnel functions, $f(X)$ and $g(X)$ (Abramowitz and Stegun 1964, p300, eqns 7.3.5 and 7.3.6), as follows:

$$A_D(X) = \mathrm{sgn}(X)\left[f(|X|) - \mathrm{i}g(|X|)\right], \quad (7)$$

Plots and asymptotes of the functions $f(X)$ and $g(X)$ can be found in Pierce[28], which demonstrate their most important properties that $f(0) = g(0) = 1/2$, $f'(X)$, $g'(X) < 0$ for $X > 0$ and $f(X) \sim (\pi X)^{-1}$ and $g(X) \sim \pi^{-2}X^{-3}$ for large X; practically, these asymptotes are accurate so long as X is larger than 2. The theoretically obtained insertion loss for our thin vertical screen straight top (S) can now be derived analytically as

$$\mathrm{IL_{th}}(\theta_S,\theta_M,f,R,C) = \\ -20\log_{10}\left|\frac{\sqrt{1+\cos(\theta_S+\theta_M)}}{2}\left[A_D\left(\sqrt{\frac{4fR}{C}}\cos\left(\frac{\theta_S-\theta_M}{2}\right)\right)+A_D\left(\sqrt{\frac{4fR}{C}}\sin\left(\frac{\theta_S+\theta_M}{2}\right)\right)\right]\right|. \quad (8)$$

We note here that the important response of insertion loss to distance R, sound speed C and frequency f only appears as the product fR/C, confirming the ability of our scaled lab experiments to reproduce the effect of a full size non-absorbing barrier. The consequence also highlights the fact that increasing the distance of the microphone and point source from the top of the barrier by some factor achieves an equivalent increase in insertion loss that would occur by increasing the frequency of the point source by the same factor.

The same analytical theory can also be applied to the other homogeneous tops (T, LD and LU) by adopting the theory of double-edge diffraction over multiple wedges and, in this paper, the theoretical insertion loss for the T-top is calculated using Eqs. (20) to (25) of Pierce[28] where β_S and β_L are set to 2π for the T-top. These theoretical insertion loss functions are compared directly in Section V. to the results obtained from our laboratory experiments.

IV. Results of selected experiments and general sound characteristics

In this section we consider some results from the laboratory measurements. Initially, we present the results obtained in a set of experiments conducted with the geometry S30M00R30 (see Fig. 5). Typical free and diffracted sound pressure signals as well as their spectra and insertion loss functions are presented. We consider first experimental data for the homogeneous barrier tops (S, T, UL, UD) and compare them to the case of the free signal (F). After that similar data for the heterogeneous jagged tops (RG, RN) are considered. In both cases the results obtained by using both Fourier analysis and a 1/3rd octave filter are presented and compared.

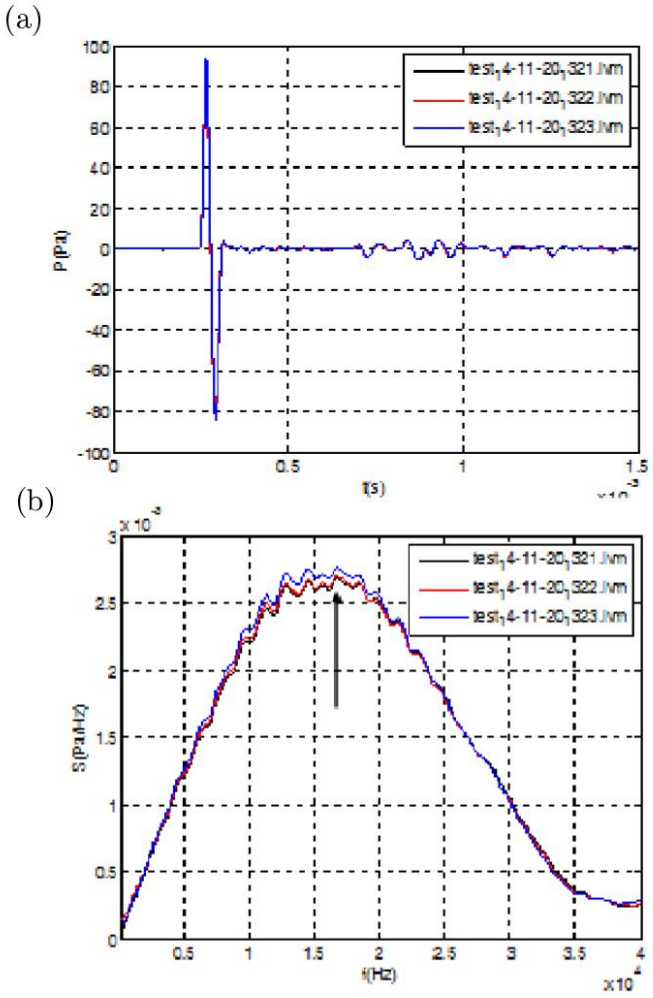

Figure 6: (a) A succession of three recordings of the sound pressure signal, $P(t)$, as a function of time, t, for three free (F) signals (see the legend) in the S30M00R30 configuration. All three signals practically coincide, and resemble the so called N-wave with a weak tail. (b) spectral density amplitude, $S(f)$, as a function of frequency, f, for the three free (F) signals. As can be seen, all three spectra also practically coincide. The arrow shows the dominant frequency, which was estimated from the data to be $f_0 = 17$kHz.

A. Free signal (F)

Three recordings of pressure, $P(t)$, measured at the microphone as a function of time, t, for three free (F) signals are shown in Fig. 6(a). All three signals practically coincide, and resemble the so-called N-wave with a weak tail; this is a profile that is typically used in acoustics to model explosions. The main signal excursion is about 80 Pa and its duration is about 60μs, suggesting an estimate of $f_0 = 17$kHz for the characteristic frequency. Three frequency spectra, calculated using a fast Fourier transform (FFT) on the three signals shown in Fig. 6(a), are shown in Fig. 6(b). The estimated characteristic frequency is shown here by the arrow and lies close to the frequency of the spectral maximum. The dominant frequencies of the signal are an order of magnitude higher than the dominant frequencies of typical traffic noise[10,32]. Thus, in our experiments the scaling factor[16] of 1:10 seems appropriate. The spectrum obtained from an average of the pressure recordings taken for the free (F) case is used below to calculate the barrier insertion losses as functions of frequency.

B. Homogeneous tops (S, T, LU, LD)

The spectral density of the mean diffracted signal for the barriers with homogeneous tops in the configuration S30M00R30 are shown in Fig. 7. For the thin vertical screen (S), the max amplitude of the recorded diffracted signal is about 15 Pa, which is approximately six times less than the free (F) signal measured with no barrier (Fig. 6). In addition, the spectral maximum amplitude for diffracted signal for the thin vertical screen (S) top is 4 kHz lower compared to the recorded free (F) signal. The spectrum of the mean diffracted signal for the T-shape (T) top is shown in Fig. 7(b). The signal is not only significantly reduced in amplitude compare to the thin vertical screen, but a noticeable secondary N-wave is present in the pressure recording. The secondary N-wave is shifted compare to the main one by approximately 0.25ms, which results in the characteristic harmonics of the

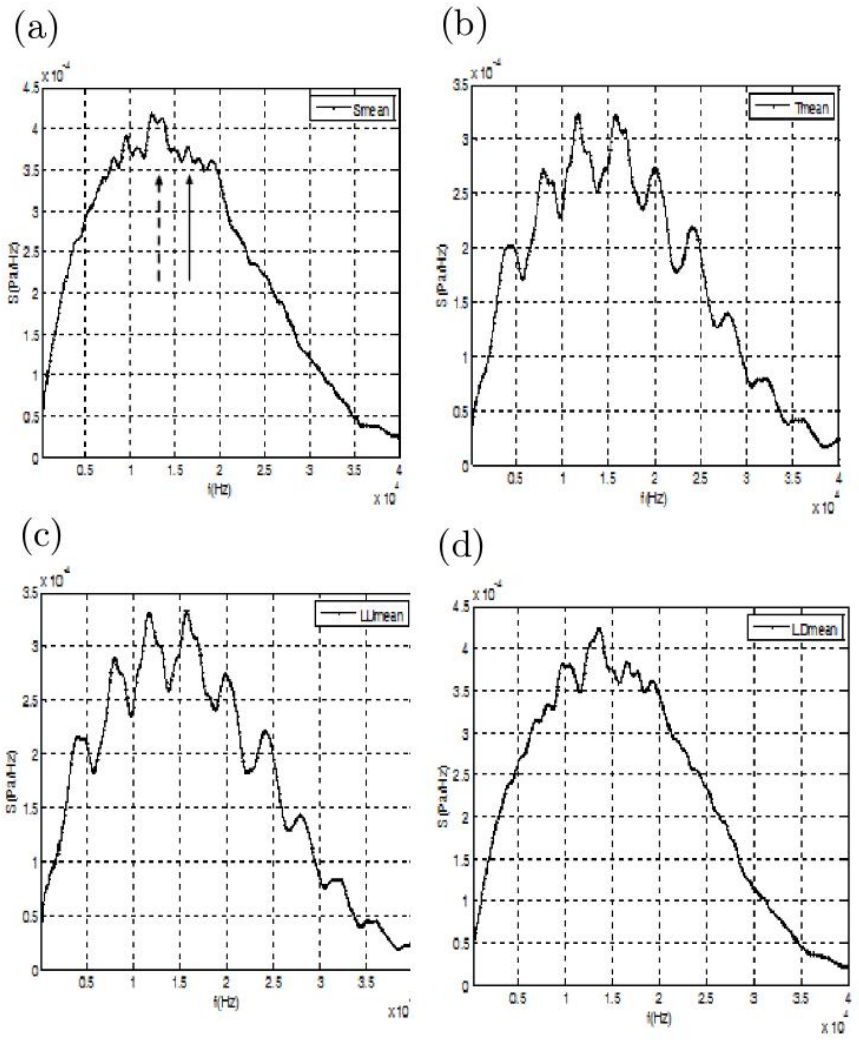

Figure 7: Spectrum density amplitudes for the mean diffracted pressure signal for the following homogeneous barrier tops: (a) thin vertical screen (S), (b) T-shaped top (T), (c) L-shaped (LU) top and (d) L-shaped (LD) top. The solid arrow shows the estimated characteristic frequency of the free signal and the dashed arrow shows the approximate position of the spectral maximum.

main frequency 1/(0.25 ms)=4 kHz that can be observed in the spectrum.

For further comparison, the spectra of the mean diffracted sound signals for the L-shape tops extending towards the source (LU) and away from the source (LD) are shown in Figs. 7(c) and (d) respectively. The spectrum for the LU top is qualitatively very similar to the spectrum shown in Fig. 7(b) for the T top. More detailed analysis shows that the LU top pressure data, for signal as well as for spectrum, are somewhat higher than similar data for the T top. On the other hand, the spectrum for the LD top is qualitatively very similar to that of the thin vertical screen (S) top in Fig. 7(a). These similarities are likely to be caused by the fact that, in the case shown, the microphone is located at the same height as the barrier top ($\theta_D = 0$) and so the main diffractive effect arises from the shape of the edge facing the source.

C. Heterogeneous tops (RG, RN)

In contrast to the diffracted signals from the homogeneous tops, the diffracted signals from the heterogeneous (jagged) tops depend strongly on the along-barrier position. As mentioned above, the diffracted signals from the heterogeneous tops, which include jagged regular (RG) and jagged random (RN) top geometries, were measured at 17 different lateral positions for each heterogeneous top. Strong amplitude and phase variability of signals (as well as the resulting spectra) is apparent from the pressure recordings $P(t)$ at each lateral position (not shown). These signals not only have different amplitudes of the leading N-waves, but positions of the following local extrema are also different. However, taking into account that the typical length scale of the barrier top variation is relatively small, in practice, compared to the distance from the barrier top to the source and microphone, the exact sound characteristics at specific locations relative to the along-top coordinate are not very important. Of more practical interest is the averaged, over this relatively small length scale, sound characteristics. As the averaging of all recorded

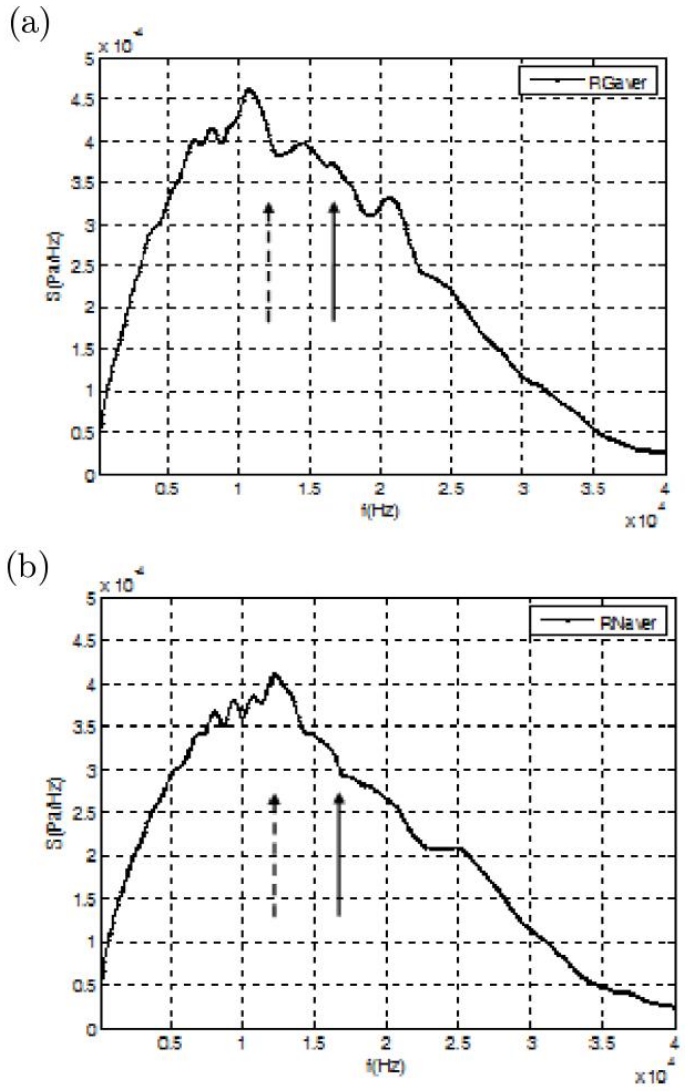

Figure 8: Spectrum density amplitudes for the mean diffracted pressure signal for (a) the RG jagged regular barrier top and (b) the RN jagged random barrier top. The mean is based on 17 measurements at different lateral positions as described in the text. The solid arrow shows the estimated characteristic frequency of the free (F) signal and the dash arrow shows the approximate position of the spectral maximum in each case.

pressure signals masks the individual frequency content and spectrum, instead, for each pressure signal the corresponding spectrum was calculated and an average of the 17 spectra was calculated for RG and RN barrier tops. These average spectra are shown in Fig. 8. In both cases, RG and RN, the approximate spectral maximum amplitude is approximately 12 kHz lower than the estimated characteristic frequency f_0 of the free (F) signal. From the preliminary analysis above, the following hierarchy of the increasing barrier top efficiency may be expected: S, LD, LU, T for homogeneous tops and RG, RN for jagged tops. More accurate estimates are given below.

V. Barrier efficiency

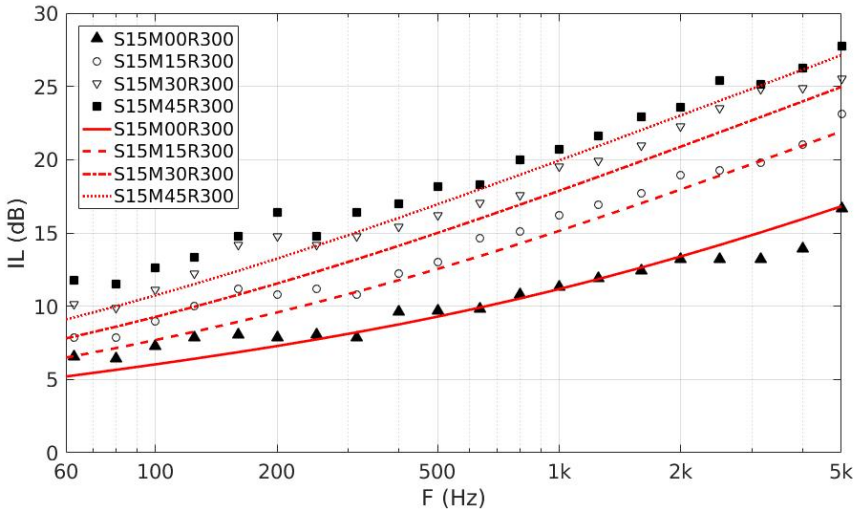

Figure 9: Symbols - Insertion losses calculated from 1/3rd-octave lab experimental data for a thin vertical barrier with a straight top (S) for four cases with different microphone positions. Red Lines - Insertion losses calculated from the analytical expression (8) using geometrical theory of diffraction.

A. Insertion loss functions for different tops

Using the spectral density amplitudes, obtained for the free and for the diffracted signals, insertion losses were calculated using (1) and typical insertion losses as functions of frequency for different top geometries are discussed briefly below. To validate our laboratory results, a plot of the insertion losses calculated from laboratory measurements for the S type barrier top lab versus the analytical expression given in (8) is shown in Fig. 9; the agreement is very good.

As a further example of the data obtained, insertion loss, IL, as a function of laboratory frequency, f, for all the laterally homogeneous barriers (S,T,LU and LD) relative to the free signal (F) for the configuration S30M00R30 is shown in Fig. 10. The results obtained from FFT calculations are shown in the top graph whereas the results of the 1/3rd octave filter calculations are shown on the bottom graph. Some variability in the FFT data at high frequencies is related to the constant spectral window width, 100Hz, which becomes small at high frequencies and the resulting 'noise' is noticeable. In the 1/3rd octave filter calculations the window width is proportional to the central filter frequency and increases with the frequency and, thus, there is no such *noise*. Despite this, both FFT and 1/3rd octave filter calculations remain satisfactorily in agreement with important details including numerous local maximums and minimums lying within ±2 dB at similar frequencies.

To compare with theory, the thick dotted line in Fig. 10 shows Maekawa's estimate (4) and the two thin solid lines in the same figure show the predictions from the geometrical theory of diffraction for a thin vertical screen and a T-top shaped barrier. As observed in Fig. 9, the agreement of both FFT and 1/3rd octave filter calculations for the thin screen S-type barrier with the geometrical theory of diffraction prediction $\mathrm{IL_{th}}$ given by (8) is excellent, especially in the range $f = 5$–25 kHz that represents the most crucial

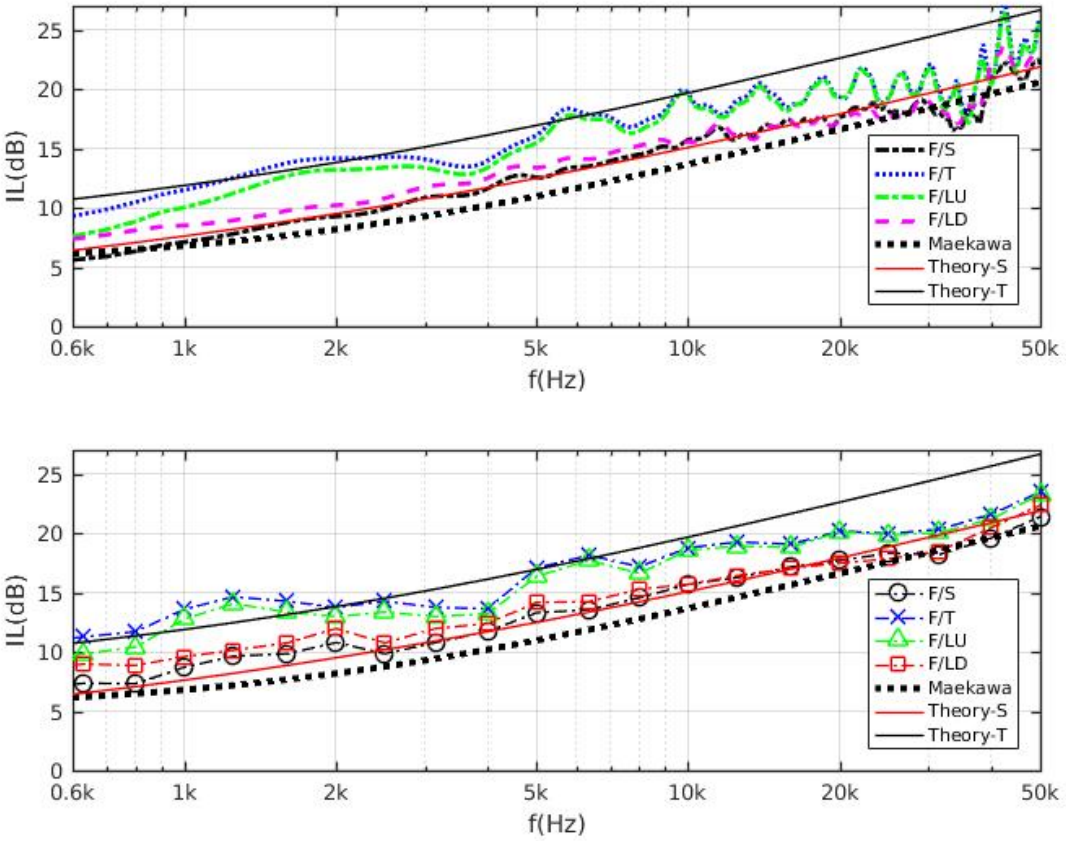

Figure 10: Insertion loss, IL, as a function of laboratory frequency f for the laterally homogeneous barriers including a thin screen (S), a T-shaped top (T) and L-shaped tops (LU and LD) relative to the free signal (F). Top - results from FFT computations. Bottom - 1/3rd octave filter calculations. The predictions from Maekawa's IL estimate for a thin screen and geometrical theory of diffraction results for a thin screen and T-top are also shown.

range of full size frequencies for traffic noise (500Hz to 2.5kHz). We note that Maekawa's estimate, while qualitatively similar, tends to underpredict the insertion losses measured in the lab by 1-2dB. For the T-top barrier, the comparison between geometrical theory of diffraction and experiments is reasonably good, but not as good as the agreement for the thin vertical screen. Both the FFT and 1/3rd octave spectra for the T-top barrier appear to undulate by roughly ±2dB above and below the theoretical line with the theoretical model tending to overestimate the insertion loss at the higher end of the spectrum.

A visual comparison of the insertion loss spectra for different barrier types in Fig. 10 and across the other tested configurations clearly indicate the T-top providing the best performance, closely followed by the LU-type barrier. The LD-type barrier performance aligns more closely with that of the thin vertical screen (S). The relative efficiency of these barrier types relative to a thin-screen S-type barrier in three different configurations is shown in Fig. 11. In all three configurations, the T-top clear has the highest efficiency followed by LU and then LD and S. Interestingly enough the LU only becomes comparable in performance to the T-top in the M00 case, where the microphone is at the same height as the barrier. The LU top's efficiency is reduced considerably for the two other cases where the microphone lies below the barrier top. For S30M00R30, geometrical theory of diffraction predicts an increase in insertion loss of 4-5dB at all the frequencies for the T-top relative to the thin screen (S) but the lab experiments suggest the performance improvement varies between +2 and +5dB across the chosen frequency range.

Typical data for the insertion loss functions for heterogeneous (RG, RN) tops relative to the thin vertical screen (S) for two particular source-microphone configurations are also shown in Fig. 11. These configurations, along with the other configurations, appear to show that the RG-top barrier does not appear to significantly improve barrier performance compared to the thin vertical screen. Some slight improvements, mainly within +1 dB but

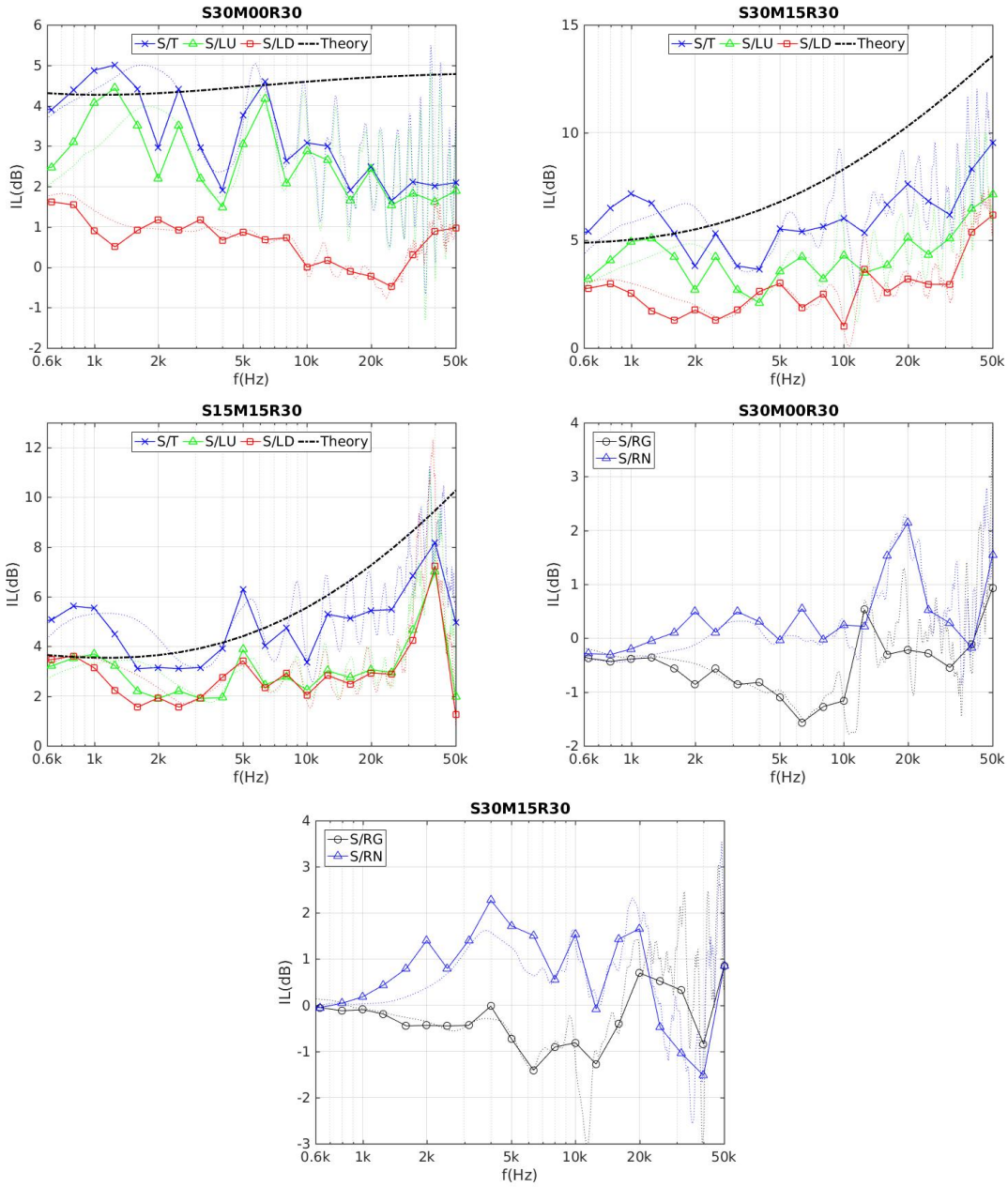

Figure 11: Insertion loss, IL, as a function of laboratory frequency f for the T-shaped top (T), the L-shaped tops (LU and LD) and the laterally heterogeneous tops (RG and RN) relative to the thin screen barrier (S) for different configurations of source and microphone positions. Faint lines show FFT results. Predictions from the geometrical theory of diffraction for the relative insertion loss of a T-top barrier relative to a thin screen are also shown.

up to 2dB for some higher frequencies, are observed for the RN top but its performance remains far below that achieved by the T-top barrier.

For all sixteen source and microphone configurations considered, similar results were obtained (see Table 1 below). A qualitative analysis, similar to that used above, suggests that the agreement between FFT and 1/3 Octave filter calculations remains satisfactory in all configurations and that the most effective barrier type tested appears to be the homogeneous T-top barrier. Furthermore, both laterally heterogeneous jagged barriers appear less effective than the T-top, with the RN-top performing somewhat better than the RG-top. To arrive at a more quantitatively definitative conclusion on barrier efficiency from the insertion loss spectra alone, however, is problematic because, in general, the insertion loss functions (2) depend on too many external parameters: in particular on the lateral position x and the frequency f. There is already an averaging of the diffracted spectra over the lateral x-axis for jagged tops, thus excluding x from the external parameters. However, a further reduction of parameters is needed. The use of a form of weighted-frequency averaging allows us to additionally exclude the frequency f from the external parameters and characterize the barrier efficiency by a so-called single number insertion loss rating. A derivation of this single number insertion loss rating is discussed below in the next section.

B. Single number insertion loss rating

The single number insertion loss $\mathcal{N}$ for a traffic barrier can be estimated as follows. The insertion loss spectrum, $IL(f)$, as measured in the scaled $(1:10)$ laboratory experiments, is rescaled from the laboratory frequencies, f, to the field frequencies, $F = f/10$, as $IL(F) = IL(f/10)$. A suitable empirical or analytical profile for a typical A-weighted traffic noise spectrum $S(F)$ is then adopted. In the estimates provided below we use the internationally standardised traffic noise spectrum given by European standard EN 1793-3[32,33]. A single number insertion loss rating, $\mathcal{N}$, (or barrier efficiency) in decibels for

each barrier type can be calculated as follows[33]:

$$\mathcal{N} = 10 \log_{10} \frac{\sum_{i=n}^{m} 10^{S(F_i)/10}}{\sum_{i=n}^{m} 10^{S(F_i)/10 - IL(F_i)/10}}, \tag{9}$$

where n and m are the lowest and higher indices taken for the 1/3rd octave band central frequencies, F_i, that are of practical significance (for EN1793-3 the applied range is 100Hz to 5kHz).

After employing this procedure, as well as the above-mentioned averaging over the lateral x-axis, the number of parameters in (2) can be reduced from six to four $IL(F, R, \theta_S, \theta_M, A, x) \rightarrow \mathcal{N}(R, \theta_S, \theta_M, A)$, and the data on $\mathcal{N}$, obtained from the results of all 112 experiments, are presented below. Recall that for field estimates, the lab frequencies f must be divided by ten and any lengths, *e.g.* R, should be multiplied by ten. To further confirm the robustness of the procedure, single-number insertion loss ratings were also calculated using a second traffic-noise spectrum standard from the Acoustical Society of Japan[10] and broadly similar $\mathcal{N}$ values and trends were obtained in this case.

VI. Directivity diagrams for single number insertion loss ratings

The values obtained for $\mathcal{N}$ from our experiments are summarized in Tables I and II. Table I shows the single number insertion loss ratings for all barrier types (S, T, LD, LU, RG, RN) relative to the free (F) signal for all selected configurations of source and microphone position. Table II then shows the single number insertion loss ratings for the homogeneous barrier types T, LD and LU relative to both the free (F) signal and the thin vertical screen (S). Recall, that the notation $\mathbf{S}\theta_S\mathbf{M}\theta_M$ is used. Also, note that the relative values for $\mathcal{N}$, given in Table II, are not simply the differences of $\mathcal{N}$ values from Table I, but the result of separate calculations using different relative insertion losses in (9). The results are discussed below.

Table I: Single number insertion loss ratings, $\mathcal{N}$, relative to the free signal (F) as estimated for various barrier top in different source-microphone positions.

Config	F/S	F/RG	F/RN	F/T	F/LU	F/LD
R=300cm						
S15 M00	10.8	9.8	10.7	12.9	12.5	10.9
S15 M15	14.8	14.1	15.2	19.0	17.4	17.2
S15 M30	17.9	16.9	18.2	22.7	21.9	21.8
S15 M45	19.4	19.2	20.4	25.9	23.1	24.0
S30 M00	14.2	13.4	14.6	17.4	16.9	14.8
S30 M15	17.1	16.5	18.1	22.4	20.7	19.2
S30 M30	19.7	19.1	20.4	26.0	23.3	22.7
S30 M45	21.2	21.3	24.4	29.8	26.1	26.7
R=450cm						
S15 M00	12.0	11.2	12.1	13.5	13.2	12.4
S15 M15	15.9	15.1	16.3	19.5	17.9	17.6
S15 M30	19.1	19.1	19.7	24.4	21.8	22.4
S15 M45	20.6	20.8	21.5	27.1	23.5	25.1
S30 M00	15.7	14.7	16.1	17.8	17.8	15.8
S30 M15	18.6	18.6	19.4	23.4	22.1	21.0
S30 M30	21.0	21.2	21.5	26.4	24.9	24.5
S30 M45	22.5	23.4	25.1	31.7	28.4	28.6

Table II: Single number insertion loss ratings, $\mathcal{N}$, relative to either the free signal (F) or to the thin screen barrier (S) as estimated for homogeneous barrier tops T, LU and LD in different source-microphone positions. Two values of $\mathcal{N}$ are given in each cell corresponding to two different values of R: the first number is for $R = 300$cm, the second number is for $R = 450$cm.

Config	F/T	F/LU	F/LD	S/T	S/LU	S/LD
S15 M00	12.9-13.5	12.5-13.2	10.9-12.4	2.1-1.5	1.8-1.2	0.1-0.2
S15 M15	19.0-19.5	17.4-17.9	17.2-17.6	4.6-3.9	2.8-2.2	2.6-1.9
S15 M30	22.7-24.4	21.9-21.8	21.8-22.4	5.3-6.1	3.9-3.0	4.1-3.8
S15 M45	25.9-27.1	23.1-23.5	24.0-25.1	6.6-6.5	4.2-3.1	4.6-4.7
S30 M00	17.4-17.8	16.9-17.8	14.8-15.8	2.8-1.7	2.4-1.9	0.3-0.0
S30 M15	22.4-23.4	20.7-22.1	19.2-21.0	5.7-5.3	3.9-3.8	2.4-2.9
S30 M30	26.0-26.4	23.3-24.9	22.7-24.5	7.1-5.7	3.6-4.3	3.1-4.1
S30 M45	29.8-31.7	26.1-28.4	26.7-28.6	9.6-9.0	5.6-5.8	5.9-6.0

A. Jagged laterally heterogeneous tops - RG,RN

The data shown in Table I shows that the efficiency of RG and RN barrier types is not significantly different from that of the thin screen S-type barrier. The N values for the RG top, in average, are $0.5 - 1.0$ dB lower than the values for the S top (see the exact values of $\mathcal{N}$ in Table I). On the other hand, $\mathcal{N}$ values for the RN top appear, on average, to be no more than 1dB higher than the S top values. Thus, the use of RG and RN tops does not appear to improve significantly barrier performance. Only in the laboratory experiments with large angles, e.g. $(\theta S, \theta_M) = (30°, 45°)$, does the RN-top show a significant increase in $\mathcal{N}$, of the order $2 - 2.5$ dB, compared to the S-top.

This general conclusion does not agree well with the preliminary results reported by Ho *et al.*[34], that barriers with RN-tops are significantly more effective than the thin vertical screen S-type barriers. These particular authors conducted a few laboratory experiments on random-edge barriers and concluded that the more random the edges, the more attenuation it brings. However, the authors did not say anything about the strong sound pressure variability laterally along barrier direction (*i.e.* along the x-axis). This is an important factor, but it remains unclear at what x-values the signal and the reported insertion loss were measured in the their publication. In our approach, to smooth these variations, the along barrier averaging for the insertion loss spectra was used. Note also, that the results reported by Menounou and You[12,15] for jagged tops show only the decrease of the sound pressure peak amplitude level, compare to the S top, and its significant variation in the along barrier direction, but no data is supplied on insertion losses. The lack of sound level calculations in the above-mentioned studies has also been noted previously by Pigasse and Kragh[35].

Further analysis of the RG and RN data also shows that the single number insertion loss rating $\mathcal{N}$ in all experiments increases noticeably with the increase of the source or

microphone angles (about $2-5$ dB for each 15 degrees) and these effects are comparable in the magnitude. A much smaller increase ($1-2$ dB) is also observed with the increase of the distance from the barrier top, R, from 3m to 4.5m. This behavior mimicks the theoretical predictions of the insertion loss function for the S- top given by (4) and (8). For instance, the Fresnel number, $\mathcal{F}_N$, is proportional to the distance R defined in (5). With the increase of the source or microphone angle, as well as R, the value of $\mathcal{F}_N$ in (4) increases and this leads to the increase of the insertion loss function as well as the values of the insertion loss rating, $\mathcal{N}$.

B. Homogeneous tops - T, LU, LD

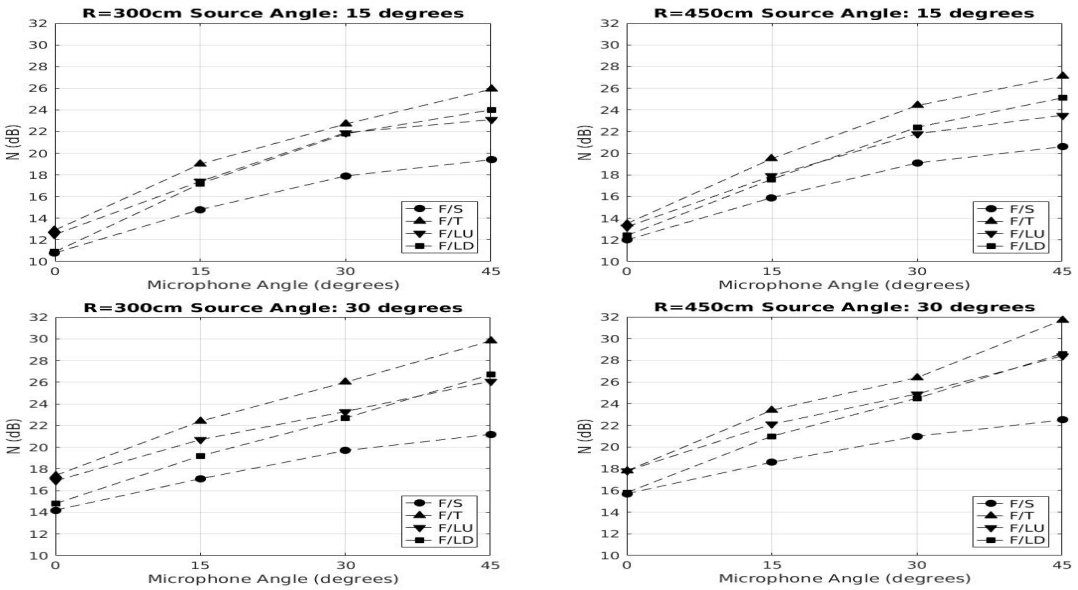

Figure 12: Directivity diagrams (relative to free F signal) for the single number insertion loss rating N as functions of microphone angle, θ_M, for different source angles θ_S and distances from barrier top R. Results for different barrier top geometries S, T, LU and LD are shown.

Directivity diagrams, relative to the free, F, signal, for the barrier top geometries S, T, LU

and LD are shown in Fig. 12. The single number insertion loss rating $\mathcal{N}$ is given as a function of the microphone angle, θ_M, for different source angles, θ_S, and two different distances from the barrier top, R. As can be seen, in all experiments the efficiency of the T top is significantly better than the other tops. For example, the $\mathcal{N}$ values for the T top (triangles), at small microphone or source angles, in average, appear to be $2.0 - 2.5$ dB higher than the values for the S top (circles - see also Table I). This difference increases noticeably up to $7 - 9$ dB with the increase of the microphone or source angles and this is broadly in line with predictions from the geometrical theory of diffraction. At smaller angles, the LD top efficiency (squares) is similar to the S-top (circles), while the LU efficiency (inverted triangles) is markedly better than the LD efficiency by about $2 - 3$ dB making it comparable in performance to the T top (triangles) (see Fig. 12 and Table I). At increasing angles, the LU top (inverted triangles) and LD top (squares) efficiencies become more comparable to one another lying approximately $4 - 5$ dB above the S top insertion loss values (circles). However, for these configuration the efficiency of LU and LD tops lie roughly $3 - 4$ dB below the T-top insertion loss values (triangles).

Thus, in all experiments the T-top barrier shows better performance than the other barrier types (see Table I). How much better depends on the barrier top type, angles of measurements and, to a lesser degree, on the distance from the barrier top. As shown in Fig 12, the single number insertion loss rating, $\mathcal{N}$, relative to the free, F, signal, increases monotonically and significantly with increasing θ_M and θ_S. To estimate the effect of the increase in R, we show in Table II relative values, compared to the free F signal and to the S-top, of the single number insertion loss rating, $\mathcal{N}$. In each column two $\mathcal{N}$ values are shown for two different distances, R. As can be seen, the effect of the distance change on $\mathcal{N}$ is small (on average about 0.5-1.5 dB) and may be neglected compared to the effect of a change in either θ_S or θ_M. This rather unexpected result is in line with the experiments of

Okubo and Yamamoto[5]. Thus, to leading order, the effect of the distance change may be neglected and the number of parameters in (2) can be reduced to only three, *i.e* $\mathcal{N}(R, \theta_S, \theta_M, A) \rightarrow \mathcal{N}(\theta_S, \theta_M, A)$, to determine a general barrier top efficiency measure, $\mathcal{N}$.

VII. Conclusions

This research was motivated by the need to develop a methodology for parsimonious scaled acoustic laboratory experiments where the acoustic characteristics of the traffic noise diffracted above sound barriers with different tops may be estimated and compared. Short impulsive spherical sound waves with a broad frequency spectrum were used in experiments as a controlled sound source. A highly stable three-electrode spark discharger was designed and constructed for this purpose. Because the duration of the sound pulse is sufficiently short, the primary signal diffracts from the barrier top and arrives to the receiver earlier than any secondary signals (*e.g.* any signals reflected from surroundings). The latter signals are ignored and only the information from the primary signal is used. This eliminates the need to use expensive acoustic anechoic chambers for experiments. The typical frequency band of the sound source (1–30 kHz) is 10 times the frequency band of typical traffic noise (100–3000 Hz), and the experiments can be considered as $1:10$ scaled experiments of real traffic sound barriers.

Numerous scaled experiments (112 in total) were conducted with different barrier tops and source-receiver positions. Homogeneous barrier tops that possess no variation of geometry laterally along the barrier, as well as heterogenous jagged tops that do were considered. The results of measurements were processed by using the spectral analyses of the free and diffracted signals. First, frequency spectra were calculated and then the insertion loss spectral functions were estimated for different source-receiver positions and barrier top geometries; these insertion loss functions were subsequently analyzed. Two different methods were used to calculate frequency spectra, namely, Fourier transforms and

a 1/3rd octave filter. Both methods demonstrate satisfactory agreement for all experiments but with an advantage of the 1/3rd octave filter being that its spectrum is less noisy. The experimental data was also validated against theory with very good agreement for a thin vertical screen when compared to a prediction using the geometrical theory of diffraction. However, when the same theoretical approach was applied to a T-top barrier the agreement was not quite good with variations of $1-2$dB between theory and experiments along with a distinct overprediction by the theory of the insertion loss at higher frequencies.

Taking into account the large number of the external parameters and to simplify the analyses, spatial and spectral averaging were applied to the data and the number of external parameters was reduced. The results obtained were rescaled to traffic barriers and, for a typical A-weighted traffic noise spectrum, weighted mean values of the traffic barrier efficiency (a single number rating) were estimated and compared. The main results of this study may be briefly formulated as follows.

A methodology has been developed which enables one to conduct, in a relatively short period of time, a large number of scaled experiments on sound diffraction from a traffic barrier top of arbitrary geometry. Detailed and accurate sound characteristics, *e.g.* spectra, insertion loss functions and single number insertion loss ratings, can be obtained easily. The considered jagged regular (RG) and random (RN) tops, in general, do not appear to improve significantly the barrier performance. Only in the experiments with large microphone-source angles does the RN top show any modest increase in the single number insertion loss rating $\mathcal{N}$ compare to a thin vertical screen. This result does not agree well with previously reported results that such jagged tops are significantly more effective than thin vertical screens[12,15,34]. These authors, however, did not consider the spectrum variability laterally along the barrier. In our approach, this was taken into account and lateral avaeraging of the insertion loss functions along the barrier was used resulting in

relatively low differences in $\mathcal{N}$ values compared to a thin vertical screen. Some of the considered homogeneous tops (T, LU, LD) showed in general significantly better efficiency compare to the thin vertical screen. The best performing appears to be the T top, follow by LU and LD tops. In all cases, the single number insertion loss ratings, $\mathcal{N}$, increase monotonically and significantly (up to 20 dB) with an increase in the angles of sound source and microphone position. In comparison, the effect of the change in microphone and source distance from the barrier top, R, on $\mathcal{N}$ is relatively small (on average about $0.5 - 1.5$ dB) and may therefore be neglected when compared to the effect from a change in angle. This result is in line with previous experiments[5].

Finally, note that parameterizations and/or improved theoretical considerations, similar to (4) and (8) for the thin vertical screen, are obviously needed for other barrier tops. However, this requires conducting a larger number of experiments with differing top geometries. Using the methodology developed and presented here, we plan to work in this direction in the future.

Acknowledgements

This research was supported by a Arizona Department of Transportation Research Center award (SPR-699) to University of Notre Dame through Illingworth-Rodkin Inc. We are most grateful to Senior Res. Eng. Scott Coppersmith for his assistance in the design and construction of the spark discharger. We are also grateful to Mr. Santiago Espinosa for his help in writing the package of MATLAB programs and last, but not least, to Mr. Patharapong Bhuripanyo for his immense help in data processing and analysis.

Appendix A. MATLAB programs

The pressures signals obtained from the memory of the digital oscilloscope (see Fig.1) were stored as ".lvm" files using LabVIEW software. To process these data, a custom-built MATLAB software package was used. The program collects the sound pressure signals directly from the ".lvm" files generated by LabVIEW and, to process the initial data, some parameters from the user are required, e.g., oscilloscope sensitivity, time scale, amplification of the preamplifier. The code is used to convert the initial data from these files into a format acceptable to MATLAB. Then the initial pressure signals are graphed, analyzed visually, to exclude obviously erroneous measurements, and processed to obtain the desirable acoustic characteristics, including the frequency spectra, relative insertion loss functions and single number insertion loss ratings. The code is divided into a main program named the "control panel" and supporting programs which are used to calculate the "processing functions" for different barrier top geometries and microphone-source positions. The free signal (no barrier), as well as signals diffracted by different barrier tops, are used in the calculations. The processing functions transform the initial oscilloscope voltage values into the sound pressure and these are used to calculate the appropriate spectra. The main control panel program then collects the relevant information from all processing functions and inputs it into the corresponding spectra analyses. For comparison, two different methods were used to calculate the frequency spectra from the initial data, namely, a standard fast Fourier transform and a 1/3rd octave filter. Additional functions are used to calculate relative insertion losses for each type of tops from the corresponding power spectra and to graph the relevant information. The 1/3rd octave filter was originally designed for MATLAB by Dr. Christophe Couvreur[24] and this code was modified to cover the higher frequency band (up to 80 kHz) required here by Dr. Tamas Zsedrovit. The measured pressure wave signals were input directly into the filter. A "filter function" and

its sub functions were then used to calculate pressure power spectra. An additional function "IL" was used to calculate insertion loss spectra for each type of barrier top from the corresponding power spectra and the relevant insertion loss function was plotted.

Appendix B. Spark Discharger

The spark gap trigger circuit was constructed using an automotive ignition coil as the high voltage source. A variable transformer was employed in this circuit to adjust the trigger voltage for repeatability and to eliminate false triggers. A 400 V TVS and a high voltage capacitor was placed in parallel with the trigger switch contacts as a "snubber" to clamp voltage spikes that could damage the switch contacts. When a pushbutton switch is closed, the automotive ignition coil is energized. When the same pushbutton is then opened, the sudden change of current flow in the primary side of the coil causes a high voltage in the secondary coil following Faraday's law of electromagnetic induction, and this is used to trigger the main spark gap by a partial ionization and breakdown of the air in the gap.

REFERENCES

[1] M. Garai and P. Guidorzi, "In situ measurements of the intrinsic characteristics or the acoustic barriers installed along a new high speed railway line.", Noise Control Eng. J. **56**(5) 342 – 355 (2008).

[2] S. M. Fard, N. Kessissoglou, S. Samuels, and M. Burgess, "A review of road traffic barriers for low frequency noise", Proceeding of Meetings on Acoustics **19**(1) 040081 (2013).

[3] D. N. May and N. M.Osman, "Highway noise barriers - new shapes", J. Sound Vib. **71**(1) 73 – 101 (1980).

[4] T. Okubo, "Edge-modified noise barrier", J. INCE Japan **28** 317 – 322 (2004).

[5] T. Okubo and K. Yamamoto, "Procedures for determining the acoustic efficiency of edge-modified noise barriers.", Appl. Acoust. **68**(7) 797 – 819 (2007).

[6] J. Parnell, S. Samuels, and C. Tsitsos, "The acoustic performance of novel noise barrier profiles measured at the roadside.", Acoust. Australia **38**(3) 123 – 129 (2010).

[7] S. R. Shaffer, *Investigations of environmental effects on freeway acoustics*, PhD Dissertation, Arizona State University, Tempe, AZ (2014).

[8] R. Seznec, "Diffraction of sound around barriers: use of the boundary-elements technique", J. Sound Vib. **73**(2) 195 – 209 (1980).

[9] D. C. Hothersall, D. H. Crombie, and S. N. Chandler-Wilde, "The performance of T-profile and associated noise barriers", Appl. Acoust. **32**(4) 269 – 287 (1991).

[10] T. Ishizuka and K. Fujiwara, "Performance of noise barriers with various edge shapes and acoustical conditions", Appl. Acoust. **65**(2) 125 – 141 (2004).

[11] S. M. Fard, N. Kessissoglou, S. Samuels, and M. Burgess, "Numerical study of noise barrier designs", Proceeding of Acoustics - Victor Harbor 17-20 November (2013).

[12] P. Menounou and J. H. You, "Design of the jagged-edge noise barrier: numerical and experimental study.", Noise Control Eng. J. **52**(5) 210 – 224 (2004).

[13] F. Koussa, J. Defrance, P. Jean, and P. Blanc-Benon, "Acoustic Performance of gabions noise barriers: numerical and experimental approaches", Appl. Acoust. **74**(1) 189 – 197 (2013).

[14] European Committee for Standardization, *EN1793-4 Road traffic noise reducing devices. Test method for determining the acoustic performance. Intrinsic characteristics. In situ values of sound diffraction*, Information on how CEN Standards can be obtained is available at http://www.cen.eu (2015).

[15] P. Menounou and J. H. You, "Experimental study of the diffracted sound field around jagged-edge noise barriers", J. Acoust. Soc. Am. **116**(5) 2843 – 2854 (2004).

[16] J. Picaut and L. Simon, "A scale model experiment for the study of sound propagation in urban areas", Appl. Acoust. **62**(3) 327 –340 (2001).

[17] M. J. R. Lamothe and J. S. Bradley, "Acoustical characteristics of guns as impulsive sources", Canadian Acoust. **13**(2) 16 – 24 (1985).

[18] A. I. Papadopoulos and C. G. Don, "A study of barrier attenuation by using acoustic impulses", J. Acoust. Soc. Am. **90**(2) 1011 –1018 (2001).

[19] G. R. Watts, D. C. Hothersall, and K. V. Horoshenkov, "Measured and predicted acoustic performance of vertically louvered noise barriers", Appl. Acoust. **62**(11) 1287 – 1311 (2001).

[20] Q. Qin and K. Attenborough, "Characteristics and application of laser-generated acoustic shock waves in air spark dischargers", Appl. Acoust. **65**(4) 325 – 340 (2004).

[21] P. Yuldashev, S. Ollivier, M. Averiyanov, O. Sapozhnikov, V. Khokhlova, and P. Blanc-Benon, "Nonlinear propagation of spark-generated N-waves in air: modeling and measurements using acoustical and optical methods", J. Acoust. Soc. Am. **128**(6) 3321 – 3333 (2010).

[22] R. E. Klinkowstein, *A study of acoustic radiation from an electrical spark discharge in air.*, Doctoral Dissertation, Massachusetts Institute of Technology. **73**(2) 195 – 209 (1974).

[23] C. Ayrault, P. Béquin, and S. Baudin, "Characteristics of a spark discharge as an adjustable acoustic source for scale model measurements.", In Acoustics 2012, Nantes, France (Société Française d'Acoustique) (2012).

[24] C. Couvreur, "Implementation of a one-third-octave filter bank in Matlab". http://citeseerx.ist.psu.edu/viewdoc/summary?doi=10.1.1.57.5728 (Last Viewed December 21, 2016).

[25] Z. Maekawa, "Noise reduction by screens", Appl. Acoust. **1**(3), 157 – 173 (1968).

[26] U. J. Kurze and G. S. Anderson, "Sound attenuation by barriers", Appl. Acoust. **4**(1) 35 – 53 (1971).

[27] U. J. Kurze, "Noise reduction by barriers", J. Acoust. Soc. Am. **55**(3), 504 – 518 (1974).

[28] A. D. Pierce, "Diffraction of sound around corners and over wide barriers", J. Acoust. Soc. Am. **55**(5), 941 – 955 (1974).

[29] A. D. Pierce, *Acoustics. An introduction to its physical principles and applications.*, (Am. Inst of Physics, New York) pp. 481 – 501 (1991).

[30] H. G. Jonasson, "Sound reduction by barriers on the ground", J. Sound Vib. **22**, 113 – 126 (1972).

[31] E. M. Salomons, "Sound propagation in complex outdoor situations with a non-refracting atmosphere: model based on analytical solutions for diffraction and reflection", ACUSTICA Acta Acustica **83**, 436 – 454 (1997).

[32] European Committee for Standardization,*EN1793-3 Road traffic noise reducing devices - Test methods for determining the acoustic performance - Part 3: Normalized traffic noise spectrum*, Information on how CEN Standards can be obtained is available at http://www.cen.eu (1997).

[33] M. Garai and P. Guidorzi, "European methodology for testing the airborne sound insulation characteristics of noise barriers *in situ*: experimental verification and comparison with laboratory data.", J. Acoust. Soc. Am. **108**(3) 1054 – 1067 (2000).

[34] S. S. T. Ho, I. J. Busch-Vishniac, and D. T. Blackstock, "Noise reduction by a barrier having a random edge profile", J. Acoust. Soc. Am. **101**(5) 2669 – 2676 (1997).

[35] G. Pigasse and J. Kragh, *Optimised noise barriers*, Danish Road Directorate, Ministry of Transport, Report 194 (2011).